THE JOURNAL OF BIOLOGICAL CHEMISTRY VOL. 290, NO. 49, pp. 29414–29427, December 4, 2015

The N-terminal Region of the Ubiquitin Regulatory X (UBX) Domain-containing Protein 1 (UBXD1) Modulates Interdomain Communication within the Valosin-containing Protein p97*

Received for publication, July 22, 2015, and in revised form, October 14, 2015 Published, JBC Papers in Press, October 16, 2015, DOI 10.1074/jbc.M115.680686

Franziska Trusch[‡1], **Anja Matena**[‡], **Maja Vuk**[§], **Lisa Koerver**[§], **Helene Knævelsrud**[§], **Paul S. Freemont**[¶], **Hemmo Meyer**[§], **and Peter Bayer**[‡2]

From [‡]*Structural and Medicinal Biochemistry and* [§]*Molecular Biology I, Centre for Medical Biotechnology (ZMB), University of Duisburg-Essen, 45117 Essen, Germany and* [¶]*Department of Medicine, Section of Structural Biology, Imperial College London, London SW7 2AZ, United Kingdom*

Background: p97 cooperates with cofactors to control various aspects of cellular homeostasis. Mutations at the interdomain interface cause a multisystem degenerative disorder.
Results: We identified three binding epitopes on p97 for the N-terminal domain of cofactor UBXD1 (UBXD1-N), including disease-associated residues. Binding reduced p97 ATPase activity.
Conclusion: UBXD1-N modulates interdomain communication and activity of p97.
Significance: The polyvalent binding mode defines a new subset of p97 cofactors.

Valosin-containing protein/p97 is an ATP-driven protein segregase that cooperates with distinct protein cofactors to control various aspects of cellular homeostasis. Mutations at the interface between the regulatory N-domain and the first of two ATPase domains (D1 and D2) deregulate the ATPase activity and cause a multisystem degenerative disorder, inclusion body myopathy associated with Paget disease of bone and frontotemporal dementia/amyotrophic lateral sclerosis. Intriguingly, the mutations affect only a subset of p97-mediated pathways correlating with unbalanced cofactor interactions and most prominently compromised binding of the ubiquitin regulatory X domain-containing protein 1 (UBXD1) cofactor during endolysosomal sorting of caveolin-1. However, how the mutations impinge on the p97-cofactor interplay is unclear so far. In cell-based endosomal localization studies, we identified a critical role of the N-terminal region of UBXD1 (UBXD1-N). Biophysical studies using NMR and CD spectroscopy revealed that UBXD1-N can be classified as intrinsically disordered. NMR titration experiments confirmed a valosin-containing protein/p97 interaction motif and identified a second binding site at helices 1 and 2 of UBXD1-N as binding interfaces for p97. In reverse titration experiments, we identified two distant epitopes on the p97 N-domain that include disease-associated residues and an additional interaction between UBXD1-N and the D1D2 barrel of p97 that was confirmed by fluorescence anisotropy. Functionally, binding of UBXD1-N to p97 led to a reduction of ATPase activity and partial protection from proteolysis. These findings indicate that UBXD1-N intercalates into the p97-ND1 interface, thereby modulating interdomain communication of p97 domains and its activity with relevance for disease pathogenesis. We propose that the polyvalent binding mode characterized for UBXD1-N is a more general principle that defines a subset of p97 cofactors.

Valosin-containing protein (VCP)[3]/p97 (also called Cdc48) is an abundant "ATPases associated with diverse cellular activities" (AAA)-type ATPase, which is involved in many pathways that ensure cellular homeostasis (1, 2). These functions include proteasome-mediated degradation of misfolded or damaged proteins, key signaling pathways, and endolysosomal sorting and autophagy (3–5). To mediate the diverse functions, p97 cooperates with distinct cofactor proteins in different processes (1, 6, 7). Around 30 cofactors have been identified that bind p97 via specific interaction domains (UBX, UBX-like, PUB, and PUL) or linear motifs (VIM, SHP box, and VCP-binding motif) and serve as substrate adapters, targeting factors, or modulators of p97 activity (4, 6, 7).

p97 is considered a "protein segregase" that structurally reorganizes proteins and separates them from binding partners or cellular structures (3, 8). It acts as a macromolecular complex with its protomers building up a hexameric barrel structure. The two ATPase domains (D1 and D2) form two concentric

* This work was supported by Deutsche Forschungsgemeinschaft Collaborative Research Centre 1093 (to P. B. and H. M.). The authors declare that they have no conflicts of interest with the contents of this article.
[1] Present address: Inst. for Medical Sciences, University of Aberdeen, Foresterhill, AB25 2ZD Aberdeen, Scotland, UK.
[2] To whom correspondence should be addressed: Structural and Medicinal Biochemistry, Centre for Medical Biotechnology (ZMB)/Faculty of Biology, University of Duisburg-Essen, Rm. S03 S01 A35, Universitätsstrasse 1-5, 45141 Essen, Germany. Tel.: 49-201-183-4677; Fax: 49-201-183-4188; E-mail: peter.bayer@uni-due.de.

[3] The abbreviations used are: VCP, valosin-containing protein; UBX, ubiquitin regulatory X; PUB, peptide *N*-glycosidase/ubiquitin-associated; CAV1, caveolin-1; p97-D1D2, D1D2 domain of p97; p97-N, N-domain of p97; UBXD1, ubiquitin regulatory X domain-containing protein 1; UBXD1-N, N-terminal region of UBXD1; VIM, VCP-interacting motif; fw, forward; rv, reverse; Bis-Tris, 2-[bis(2-hydroxyethyl)amino]-2-(hydroxymethyl) propane-1,3-diol; HSQC, heteronuclear single quantum coherence; het-NOE, hetero-steady-state NOE; ATPγS, adenosine 5′-*O*-(thiotriphosphate); H, helix; L, loop.

rings, and the peripheral N-domain is coplanar with or slightly above the D1 domain, depending on the nucleotide state of the ATPase domains (9, 10). Substrate adapters and other cofactors bind either to the N-domain or the C-terminal tail of p97, depending on their binding domains (7). How force is transmitted onto substrate proteins is unclear so far, but it involves movements of the N-domains relative to the D1 ring. N-domain motions are coupled to ATP hydrolysis in D2 through a chain of conformational changes that are transmitted along the D1D2 linker, the D1 domain, and the ND1 linker (9, 11).

Whereas VCP/p97 knock-out is embryonic lethal, missense mutations in the ND1 interface cause systemic late onset degenerative disorders in humans called inclusion body myopathy associated with Paget disease of bone and frontotemporal dementia/amyotrophic lateral sclerosis that affect muscle, bone, and cortical and motor neurons (12, 13). The exact pathogenesis is unclear so far, but the prominent feature of affected tissues and tissue culture cell models includes defects in the endolysosomal system with impaired endosomal trafficking of caveolin-1 (CAV1) and autophagosome maturation (4, 5, 14, 15). Intriguingly, disease-associated mutations all cluster at the ND1 interface, consistent with deregulated ATPase activity (11, 16–18). Moreover, the mutations cause unbalanced cofactor interaction including the loss of UBXD1 binding (14, 19). As UBXD1 is involved in p97-mediated endosomal sorting of CAV1 and affected by p97 mutations (14), UBXD1 is likely directly connected to the pathogenesis. Additionally, UBXD1 is unusual among the p97 cofactors as it binds p97 in two regions, at the p97 C terminus via a PUB domain and at the p97 N-domain with a short linear interaction motif termed VIM; an additional UBX domain, which usually binds the N-domain of p97, is not functional (20).

During our cell biological studies of respective binding domains, we noticed that additional moieties in the N-terminal region of UBXD1 (UBXD1-N) are involved in targeting UBXD1 to p97 on CAV1-containing endosomes. We therefore analyzed the solution structure of UBXD1-N and its interaction with p97. We discovered a yet unappreciated second binding site for UBXD1-N on the p97 N-domain including the ND1 linker. Moreover, we found that UBXD1-N also binds the D1D2 barrel. Interestingly, we observed a modulation of the p97 ATPase activity by UBXD1-N, indicating that UBXD1-N fixes the N-domain of p97 (p97-N) in a "down" position and concomitantly favors a more compact conformation for p97. Among the residues in the N-domain of p97 targeted by UBXD1-N are critical amino acids frequently affected by disease-associated mutations, suggesting that the specific binding mode of the UBXD1 cofactor to p97 may explain the compromised function of the p97·UBXD1 complex in the context of the disease.

Experimental Procedures

Cell-based Experiments—The human CAV1-HA and UBXD1-GFP constructs were described elsewhere (14, 21, 22). pEGFP-UBXD1–5xPUB-GFP was generated by QuikChange mutagenesis, resulting in the following codon changes: N184A, K193A, Y194A, K198A, and N201A in the PUB domain as described elsewhere (20). pEGFP-UBXD1-RL-GFP was mutated to code for changes R62A/L63A in the VIM as defined by Stapf *et al.* (23). The constructs coding for the different variants of UBXD1-GFP were cotransfected with the CAV1-HA construct in U2OS parental cells using the JetPrime reagent (Polyplus, Illkirch, France) according to the manufacturer's protocol. After 24 h of co-expression, cells were analyzed by immunofluorescence staining or Western blotting. Cells were lysed for analysis in Western blotting as described elsewhere (14). Antibodies used were anti-HA (Sigma), anti-GFP (Roche Applied Science), and anti-α-tubulin (Sigma). For immunofluorescence staining, cells were fixed in 4% paraformaldehyde for 20 min, immunostained with an anti-HA antibody (Covance, Munster, Germany) to detect CAV1-HA, and visualized by epifluorescence microscopy. Images were taken on a Nikon Eclipse Ti microscope with the Andor DR-328G-C01-SIL camera. Image acquisition was driven by Andor IQ software (scale bar, 10 μm).

Plasmid Constructs for Recombinant Protein Expression—Different UBXD1 constructs (amino acids 1–133, 32–133, and 1–80) and the D1D2 domain of p97 (amino acids 200–806) were cloned into a modified pET41 vector (Invitrogen) as described elsewhere (24) with an N-terminal GST tag and a PreScission protease cleavage site. Primers used were as follows: UBXD1-N(1–80): fw, 5′-CACACAGGGCCCATGAAAAAATTCTTCCAG; rv, 5′-GGTTGGCTCGAGCTTAACGGATGGTATCCTGAGATGTTG; UBXD1-N(32–133): fw, 5′-CACACAGGGCCCCACAAAGAGAAGCCGAACCAG; rv, 5′-GGTTGGCTCGAGCTTACCTCAG GGTGGCACCAG; p97-D1D2: fw, 5′-CACACAGGGCCCGAAGTAGGGTATGATGACATTGG; rv, 5′-GGTTGGCTCGAGCTTAGCCATACAGGTCATCATC. DreamTaq DNA polymerase was purchased from Thermo Scientific (Schwerte, Germany), and restrictions enzymes ApaI and XhoI (Fast Digest) and T4 ligase were from Fermentas (Schwerte, Germany). All constructs were verified by Sanger sequencing (GATC GmbH, Cologne, Germany). From previous pulldown experiments (data not shown), the construct UBXD1-N(1–133) was proven to be sufficient for p97-N binding. After nuclear magnetic resonance (NMR) titration experiments of ^{15}N-labeled UBXD1-N with p97-N, it became clear that for this interaction only residues in the first part up to Arg^{80} are needed. As high molecular weight and the resulting high rotational correlation times hamper NMR analysis, the smaller but sufficient fragment 1–80 of UBXD1-N was used for NMR studies of UBXD1-N·p97-N complex formation. The construct p97-N(1–213) was provided in a pProEx vector (Invitrogen) with an N-terminal His$_6$ tag. UBXD1 mutants (D11A/I12A and R62A/L63A) were produced with the Q5 site-directed mutagenesis kit (New England Biolabs, Frankfurt am Main, Germany) according to the user's manual. Primers used were as follows: UBXD1-N$_{D11A/I12A}$: fw, 5′-CAGGAGTTCAAAGCGGCCGCGAAGTTCAAGAGCGCC; rv, 5′-GGCGCTCTTGAACTTCGCGGCCGCTTTGAACTCCTG; UBXD1-N$_{R62A/L63A}$: fw, 5′-ACGCTCTGGCAGCGGCGGAGCAGAAACAGTC; rv, 5′-GACTGTTTCTGCTCCGCCGCTGCCAGAGCGT.

Expression of Recombinant Proteins and Cell Lysis—Expression constructs were transformed into *Escherichia coli* BL21(DE3)T1r (Sigma-Aldrich). 100 ml of overnight cultures of transformed bacteria were resuspended in 4 liters of LB

medium and grown to an A_{600} of 0.8. For isotope labeling (^{15}N and/or ^{13}C) studies, 1 liter of LB medium was inoculated with the overnight culture and grown to an A_{600} of 0.8. Subsequently, cells were pelleted by centrifugation (3,000 × *g*, 15 min, room temperature), resuspended in 4 liters of M9 medium supplemented with 1 g/liter [^{15}N]ammonium chloride and/or 4 g/liter [^{13}C]glucose, and again grown to an A_{600} of 0.8. After induction of protein expression with 250 μM isopropyl β-D-1-thiogalactopyranoside, cells were shaken further for 6 h at 30 °C for UBXD1 constructs and overnight at 30 °C for p97 constructs. For cell lysis, cells were centrifuged (5,500 × *g*, 20 min, 4 °C), resuspended in low salt buffer (20 mM Tris-HCl, 50 mM NaCl, 1 mM PMSF, pH 7.4), and frozen. After a freezing cycle, cells were incubated with 300 mg of lysozyme for 1 h at 4 °C followed by sonication. The cell lysate was ultracentrifuged (90,000 × *g*, 70 min, 4 °C), and the filtrated supernatant was used for purification.

Purification of Recombinant UBXD1 and p97 Constructs—The protein mixture containing GST-tagged UBXD1-N or p97-D1D2 protein was applied to a glutathione column (Macherey and Nagel, Dueren, Germany) in buffer 1 (20 mM Tris, 150 mM NaCl, pH 7.4) and eluted with buffer 1 additionally containing 20 mM glutathione. The GST tag was removed by PreScission protease. The UBXD1 constructs were separated from the GST tag by size exclusion chromatography (Superdex 75 26/600 column, GE Healthcare) combined with a glutathione column in phosphate buffer (50 mM KP_i, 150 mM KCl, pH 6.5). The p97-D1D2 protein was separated from cleaved GST tag by filtration with a Centricon filter unit (30,000 molecular weight cutoff, Amicon, Millipore, Darmstadt, Germany). The protein mixture containing His_6-tagged p97-N was applied to an anion exchange column (HiTrap Q HP, GE Healthcare) in buffer 2 (20 mM Bis-Tris, pH 6.6) and eluted with buffer 2 additionally containing 500 mM NaCl. Subsequently, the eluted protein was loaded onto a nickel-nitrilotriacetic acid column (Macherey and Nagel) in buffer 3 (50 mM NaH_2PO_4, 300 mM NaCl, 10 mM imidazole, pH 8.0) and eluted with buffer 3 supplemented with 500 mM imidazole by a gradient. For NMR spectroscopy, proteins were dialyzed against 50 mM KP_i buffer, pH 6.5 for UBXD1 constructs and pH 7.2 for p97 constructs, as a compromise between high ionic strength (necessary to mimic physiological conditions) and the technical requirements for spectroscopic analyses (circular dichroism (CD), NMR, and fluorescence anisotropy).

NMR Spectroscopy—NMR experiments were performed on a 700-MHz Ultrashield NMR spectrometer (Bruker, Ettlingen, Germany) equipped with a cryoprobe (Bruker Biospin). Samples were dissolved in 600 μl (90% H_2O, 10% D_2O) of phosphate buffer. Standard triple resonance spectra (CβCαCONH/HNCαCβ) were used for backbone assignment of UBXD1-N (Biological Magnetic Resonance Data Bank entry 26664) and for the complementation of the assignment of p97-N (25). According to MALDI-TOF data of UBXD1-N, up to 16 C-terminal amino acids are proteolytically degraded during purification (data not shown) and could not be observed concomitantly. A contiguous stretch between Ala^{31} and Glu^{34}, which resides within a flexible loop, also could not be detected in the spectra. ^1H-^{15}N heteronuclear single quantum coherence (HSQC) spectra for titration experiments were recorded with 24 scans and 2,048 × 256 data points for p97-N and six scans and 2,048 × 256 data points for UBXD1-N. Data were processed with Topspin 3.0 (Bruker). Titration experiments were performed at 25 °C for p97-N and 27 °C for UBXD1-N by stepwise addition of different concentrations of binding partner as indicated. Intensity changes of signals were analyzed, and ^1H and ^{15}N shifts were combined according to the following equation (26).

$$\Delta\delta_{total} = \sqrt{(\Delta\delta_H)^2 + (0.154 \cdot \Delta\delta_N)^2} \quad \text{(Eq. 1)}$$

Hydrogen bonds were estimated from a modified D_2O exchange experiment with UBXD1-N constructs (amino acids 1–80 and 32–133). Because freeze-drying is not possible for intact UBXD1-N, the sample was concentrated using a Centricon filter unit, and buffer was repetitively exchanged with 100% D_2O. For analysis of flexibility, hetero-steady-state NOE (het-NOE) spectra for UBXD1-N were recorded with the corresponding pulse program from the Bruker pulse program library. The (^1H)-^{15}N NOEs were calculated from ratios of intensities of cross-peaks in spectra measured with and without saturation.

CD Spectroscopy—CD experiments were performed on a J-170 spectrometer (Jasco). Proteins were diluted up to 0.15 mg/ml in phosphate buffer (50 mM KP_i, pH 6.5). CD spectra were recorded with 30 scans at 25 °C subtracted by the blank (buffer without protein). The content of secondary structure was analyzed using the CDSSTR tool with the reference set SMP56 (27–29).

Fluorescence Anisotropy—UBXD1-N and UBXD1-$N_{R62A/L63A}$ were labeled with $Atto_{594}$ according to the user's manual. p97-N (430 μM), p97-D1D2 (1 mM), and p97 (290 μM) were titrated in 10 steps to labeled UBXD1 constructs as indicated. The measurements were done in phosphate buffer (50 mM KP_i, 0.05% Tween, pH 7.2) at 25 °C on a Cary Eclipse fluorescence spectrometer (Agilent Technologies, Waldbronn, Germany). The curves were fitted with GraphPad Prism 5.0 using a one-site-specific binding model. All fitting curves have R^2 values between 0.93 (UBXD1-N_{WT} and p97-N) and 0.99 (UBXD1-$N_{R62A/L63A}$ and p97-D1D2).

ATPase Activity Assay—The ATPase activity of p97 was measured with an NADH-coupled ATPase activity assay as described elsewhere (11). 500 nM p97 protein (monomeric form) was incubated with several concentrations of cofactors as indicated in 100 mM Tris-HCl at 37 °C. The decrease in the NADH absorption at 340 nm due to ATPase activity of p97 was measured on a Cary 100 Bio UV/visible spectrometer (Agilent Technologies) in real time.

Limited Proteolysis—The limited proteolysis of p97 was performed with trypsin protease (molar ratio, 1:100) in the absence and presence of several cofactors. p47 is known to hold p97-N in an upper conformation, and ATPγS fixes the N-domain of p97 more above the D1 ring. Additionally, we tested UBXD1-N(1–133), which contains the p97-N binding sites in helix (H) 1/H2 and the VIM, as well as the modified construct UBXD1(32–133)$_{R62A/L63A}$, which lacks both binding sites as a p97-N non-binding control. The measurements were per-

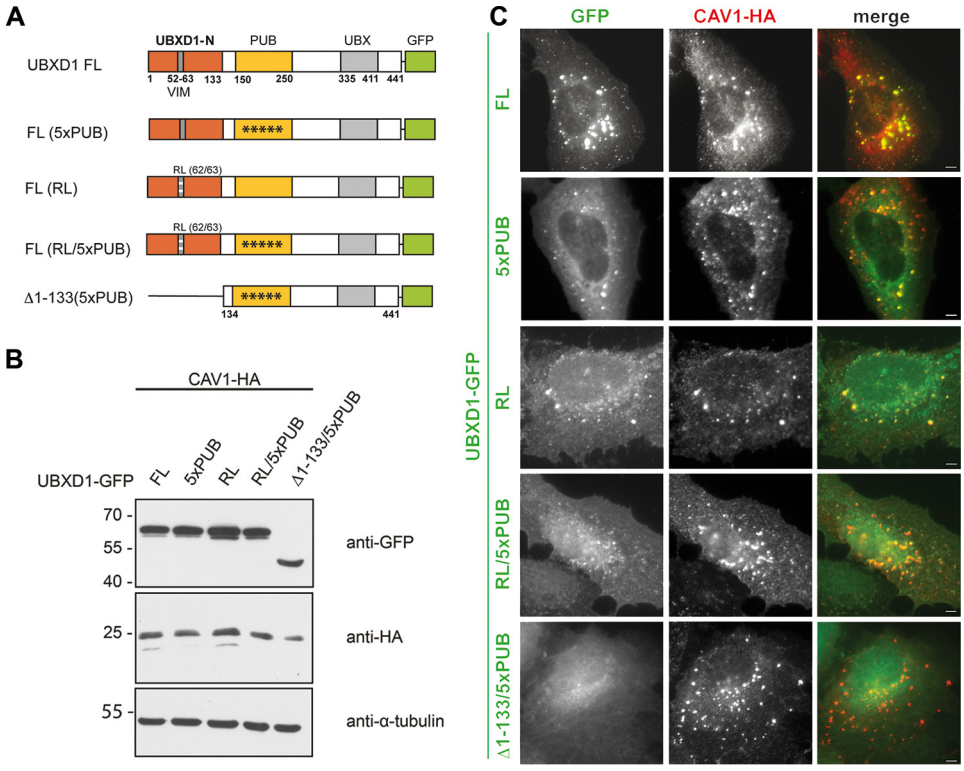

FIGURE 1. **Sequence elements of UBXD1-N outside of the VIM mediate UBXD1 targeting to p97-regulated endosomes.** *A*, schematic of UBXD1 constructs used for cell assays. To monitor UBXD1 localization in U2OS cells, cells were co-transfected with CAV1-HA and different GFP fusions of UBXD1 as indicated. The *asterisks* represent mutations. *B*, Western blot analysis of expression levels of GFP-UBXD1 variants. Indicated constructs were transiently co-expressed with HA-CAV1 in U2OS cells. Cell lysates (15 μg) were analyzed with the indicated antibodies. α-Tubulin served as a loading control. *C*, overexpression of CAV1-HA induces a p97-UBXD1-mediated response at endosomes. CAV1-HA was immunostained, and localization of different UBXD1 variants to CAV1-HA-positive endosomes was investigated. Note that endosome recruitment of UBXD1 was not affected by VIM (R62A/L63A (*RL*)) or PUB (5xPUB) mutation even in combination but was abolished by full deletion of UBXD1-N together with the PUB mutation. *Scale bars*, 10 μm. *FL*, full length.

formed in phosphate buffer (50 mM KP_i, pH 6.5) as described elsewhere (11). After a 2-h incubation at 37 °C, each sample was mixed with SDS loading buffer and loaded for SDS-PAGE.

Results

Sequence Elements of UBXD1-N Outside of the VIM Are Required to Functionally Cooperate with p97 at Endosomes—When endocytic invaginations (called caveolae) are destabilized, their major constituent, CAV1, is targeted to lysosomes for degradation (21). To mediate the process, p97 and UBXD1 are recruited to CAV1-containing endosomes, which can be stimulated by CAV1 overexpression (14, 21, 22). To analyze the structural determinants that govern targeting of UBXD1 to p97-regulated endosomes, we transiently overexpressed CAV1-HA with diverse variants of UBXD1-GFP (Fig. 1, *A* for summary schematic and *B* for expression analysis). Besides UBXD1 wild type and truncations of the N-terminal region, variants harboring two point mutations in the VIM (R62A/L63A) or five point mutations in the PUB domain (5xPUB), which were previously shown to affect respective binding activities, were investigated (20, 23). CAV1-HA was detected by immunofluorescence with HA antibodies, and colocalization of CAV1-HA and UBXD1-GFP was visualized by epifluorescence microscopy (Fig. 1*C*). UBXD1 wild type largely colocalized with CAV1 endosomes. Mutation of either the PUB domain (5xPUB) or the VIM (R62A/L63A) reduced, but did not abolish, endosome targeting. Even when both sets of mutations were combined, UBXD1 was still detectable on CAV1-positive endosomes. UBXD1 recruitment was only abolished when the PUB domain mutations were combined with full truncation of the N-terminal region covering amino acids 1–133 harboring the VIM. These data suggest a functional significance of sequence elements in UBXD1-N flanking the VIM for localization to CAV1-positive structures and indicate that they may be involved in the functional cooperation with p97.

The Isolated UBXD1-N Exhibits Four Helical Regions—Based on UBXD1 localization studies and the lack of structural studies of the whole N terminus (residues 1–154; Ref. 20), we focused on the structure of this moiety of UBXD1 (UBXD1-N). Considering the importance of the VIM (residues 52–63) in p97 binding and the N-terminal residues 1–133 in endosome recruitment, we cloned and expressed the full N-terminal domain (UBXD-N(1–154)), UBXD1-N(1–133), and a minimal construct (UBXD1-N(1–80)) including the VIM. We used the isolated UBXD1-N as a simplified but valuable representative for studying the structure and dynamics of the N-terminal region in UBXD1. The ^{1}H-^{15}N HSQC NMR spectrum of UBXD1-N(1–133) (Fig. 2*A*) showed 109 NH signals, most of which were dispersed over less than 1 ppm along the ^{1}H dimension (~7.8–8.6 ppm). Neither extension of the N terminus of UBXD1 to Val^{154} nor reduction to Arg^{80} had any apparent effect on signal dispersion, indicating that all three constructs share a common core structure. As the C-terminal residues following Arg^{80}

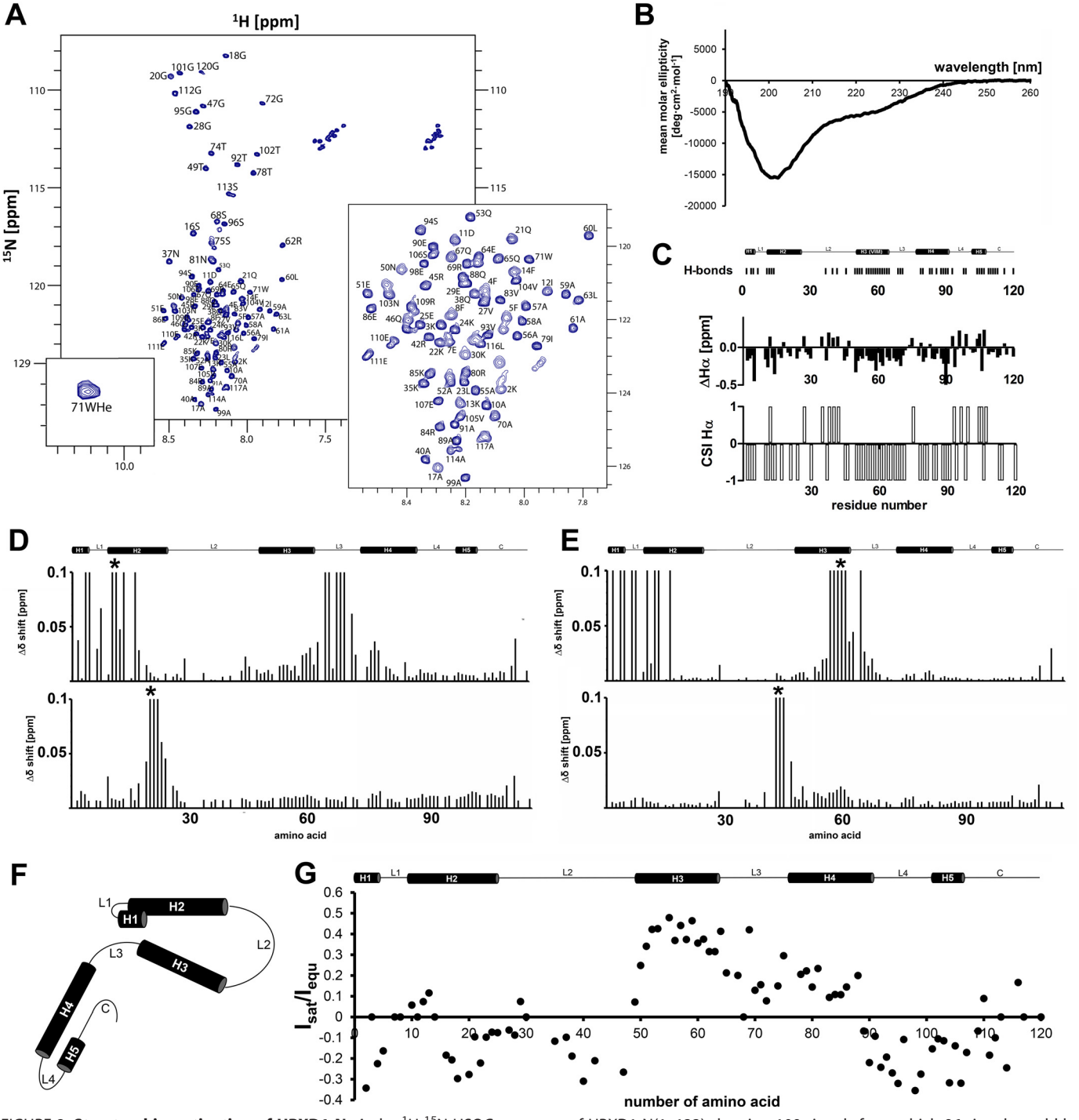

FIGURE 2. **Structural investigation of UBXD1-N.** *A*, the ^{1}H-^{15}N HSQC spectrum of UBXD1-N(1–133) showing 109 signals from which 96 signals could be assigned (50 mM KP_i, pH 6.5). An expanded region of the central portion of the HSQC spectrum is shown in the *right corner*. The NHϵ resonance of tryptophan Trp^{71} is presented in the *left corner*. *B*, CD spectrum of UBXD1-N showing an unstructured protein with α-helical character. *deg*, degrees. *C*, analysis of Hα chemical shift differences with respect to random coil values (30). Sequential crowding of positive values in the *bottom* chemical shift index (*CSI*) plot indicates helical structures. Secondary structure elements are supported by a modified D_2O exchange experiment. *D* and *E*, chemical shift difference analysis of mutants of UBXD1-N deduced from ^{1}H-^{15}N HSQC spectra of wild type and the respective mutant. The sites of mutation are indicated by *. Amide resonances of shifting residues are represented by their corresponding shift difference values. Amide resonances with chemical shift values ≫0.1 ppm are depicted as *bars* with δΔ values of 0.1 ppm for better representation. *C*, C terminus. *D*, UBXD1-$N_{D11A/I12A}$ and UBXD1-$N_{Q21A/K22A}$. In the case of UBXD1-$N_{D11A/I12A}$ (*upper* shift map) severe changes are observed in the region of the mutation H1/H2 (Lys^{2}–Ala^{17}) as well as in the region of L3 (Ala^{61}–Asn^{81}). In contrast, the mutant protein UBXD1-$N_{Q21A/K22A}$ (*lower* shift map) exhibiting the mutated residues in a random coil area only gives rise to chemical shift changes of resonances of residues around the mutated sequence position. *E*, UBXD1-$N_{R62A/L63A}$ (mutation next to L3) and UBXD1-$N_{R45A/Q46A}$. For UBXD1-$N_{R62A/L63A}$ (*upper* shift map), severe shifts are induced in the region of the mutation H3/L3 (Ala^{59}–Gln^{67}) as well as in H1/H2 (Lys^{2}–Ala^{17}). In contrast, the mutant protein UBXD1-$N_{R45A/Q46A}$ (*lower* shift map) exhibiting the mutated residues in a random coil area only gives rise to chemical shift changes of resonances of residues surrounding mutated amino acids. *F*, model of UBXD1-N implying results from chemical shift analysis, mutational studies, and hetNOE analysis. *C*, C terminus. *G*, hetNOE analysis of UBXD1-N_{WT}. ^{15}N-^{1}H heteronuclear NOEs represented by the ratio of resonance intensities I_{sat}/I_{equ} obtained from spectra recorded under saturated and non-saturated conditions. 70% of the amino acids have values <0, indicating a flexible protein (values range from −0.35 to 0.48). Amino acids with positive values correlate with the secondary structural elements H3, L3, and H4 (Thr^{49}–Ala^{89}).

TABLE 1

Long range Hα-HN NOEs depicted and assigned by the software Cyana

The quality factor (0–1) indicates the reliability of the assigned NOEs. Residues that give rise to the NOEs as well as the calculated distances of atoms are shown. Interactions between the corresponding helices are labeled by +.

Quality	Peak	Residues	Upper distance	H1-VIM	H1-H2	H2-VIM
			Å			
0.95	205	Hα Lys^{13}-H Phe^{5}	3.45		+	
0.94	292	H Ile^{12}-H Arg^{80}	3.95			+
0.86	242	Hα Arg^{80}-H Asp^{11}	3.24			+
0.78	194	Hα Arg^{80}-H Ile^{12}	4.30			+
0.68	279	Hα Lys^{35}-H Phe^{4}	4.83	+		
0.66	299	H Ile^{79}-H Phe^{4}	4.43	+		
0.48	195	Hα Arg^{62}-H Ile^{12}	4.12			+
0.35	300	H Ile^{12}-H Gln^{65}	5.50			+
0.26	305	H Leu^{63}-H Ile^{12}	4.77			+
0.12	203	Hα Ala^{70}-H Phe^{5}	3.53	+		

obviously do not influence the chemical shifts of the preceding residues 1–80, one can exclude any strong interaction between these stretches of amino acids. Based on these data and our interest in the function of UBXD1-N in endosome recruitment, we focused on the structure of UBXD1-N(1–133). Sequence-based secondary structure algorithms predicted the N terminus of UBXD1-N(1–133) to reveal a random coil fraction of 57% (42% α-helix and 1% β-sheet) (31). These predictions were also consistent with experimental data deduced from the secondary structure analysis of far-UV CD spectra of the isolated N terminus of UBXD1 (46% α-helix, 18% β-sheet, and 33% random coil; Fig. 2*B*). To obtain information on the core structure of the N-terminal domain, backbone atoms of UBXD1-N(1–133) were assigned to their corresponding NMR frequencies by means of HNCαCβ for Cα and Cβ atoms, HNCO/HN(CA)CO for CO atoms, and ^{15}N total correlation spectroscopy-HSQC spectra for hydrogen atoms of the side chains. Due to the high internal dynamics of UBXD1-N, only a few medium range NOEs characterizing α-helices (*e.g.* $\alpha H(N)_{i,i+3}$; $\alpha H(N)_{i,i+4}$, etc.) were found for helices H2 and H3. However, a sufficient amount of long range NOEs for structure calculation was generally not obtained from either two-dimensional or three-dimensional NOESY spectra. We refrained from calculating an NMR-based structure of UBXD1-N, although a few long range NOEs between the helical regions could be assigned (Table 1). Chemical shifts from Hα resonances were used to predict secondary structure elements within the protein, revealing five α-helical regions (H1, Met^{1}–Phe^{5}; H2, Ala^{10}–Ser^{25}; H3, Asn^{50}–Gln^{65}; H4, Asp^{77}–Ala^{91}; and H5, Thr^{102}–Pro^{108}) (Fig. 2*C*). The formation of secondary structure elements in H1, in the first part of H2, along H3 as well as partially in H4, and at the C terminus including H5 was also confirmed by a modified D_2O exchange experiment (Fig. 2*C*, *bars* on *top*, H-bonds). H2 may exist as a helix-turn-helix element with the turn at Lys^{15}–Ala^{17}, and H4 is only poorly defined by the experimental data. As H1, H2, and H4 are predominantly defined by characteristic Hα shift values, all three helices are considered to be transient helices. The known VIM (Ala^{52}–Arg^{62}) of UBXD1-N is a part of the well defined H3. Despite the transient character of most of the helices, the mutational exchange of amino acids D11A/I12A within H2 led to significant chemical shift changes of ^{1}H-^{15}N HSQC signals belonging to amide groups of residues of H1 as well as H3/loop (L) 3 (Fig. 2*D*). Corresponding chemical shift changes of signals of residues from H1/H2 were observed upon exchange of amino acids R62A/L63A in H3 (Fig. 2*E*), revealing an interaction between these secondary structure elements. Because NMR-based structure calculation and homology modeling were not feasible, we used the information obtained from experimental data (analysis of shifts and mutational studies) to generate an *ab initio* model for UBXD1-N (Fig. 2*F*). Although the model displays interactions of helical elements within UBXD1-N, it implies a very dynamic structure, which was confirmed when retrieving information on backbone dynamics of UBXD1-N from the hetNOE of the amide resonances (Fig. 2*G*). For rigid tumbling proteins of about 14 kDa, these hetNOE values are higher than 0.6. Low hetNOE values are correlated with high internal flexibility. About 70% of the NH groups of UBXD1-N revealed negative values, indicating high internal mobility and, hence, flexibility of the backbone. Positive values were found for H2, H3 containing the VIM, L3, and H4. Although the positive values correlated with most of the defined partially transient secondary structural elements and point toward restricted backbone motility, the overall hetNOE values were below 0.5, indicating that UBXD1-N is a flexible region lacking a rigid three-dimensional folding topology.

UBXD1-N Binds the p97-N via Two Binding Sites—Based on our cell biological experiments, we wondered whether the flexible UBXD1-N moiety is capable of interacting with the p97-N. To investigate this interaction, p97-N was added step by step to ^{15}N-labeled UBXD1-N up to a molar ratio of 1:5, respectively. The corresponding chemical shift and intensity changes of the amide signals of residues of UBXD1-N were monitored by ^{1}H-^{15}N HSQC spectra. Upon titration of p97-N to UBXD1-N, 29 amide signals lost intensity, whereas another 12 signals underwent chemical shift changes, indicating a specific interaction of both proteins (Fig. 3*A*). The affected residues accumulated within two sequential stretches of UBXD1-N comprising amino acids from Lys^{2} to Lys^{30} and Arg^{45} to Trp^{71}. The first stretch belongs to H1/H2. Upon binding of p97-N, some signals underwent mainly small chemical shift changes (Lys^{2}, Phe^{4}, Phe^{5}, Glu^{7}, Phe^{8}, Asp^{11}, and Ile^{12} of H1/L1 and Lys^{30} of H2), whereas other signals decreased in intensity and finally disappeared at higher p97-N concentrations (Phe^{14}, Ala^{17}, Gln^{21}, Lys^{22}, Lys^{24}, and Glu^{25} of H2). Amino acids belonging to the disappearing peaks occupy one side of H2, pointing toward direct involvement in binding. The second p97-N binding stretch of residues of UBXD1-N from Arg^{45} to Trp^{71} contains the VIM (Ala^{52}–Arg^{62}), which is located in H3. Most of the

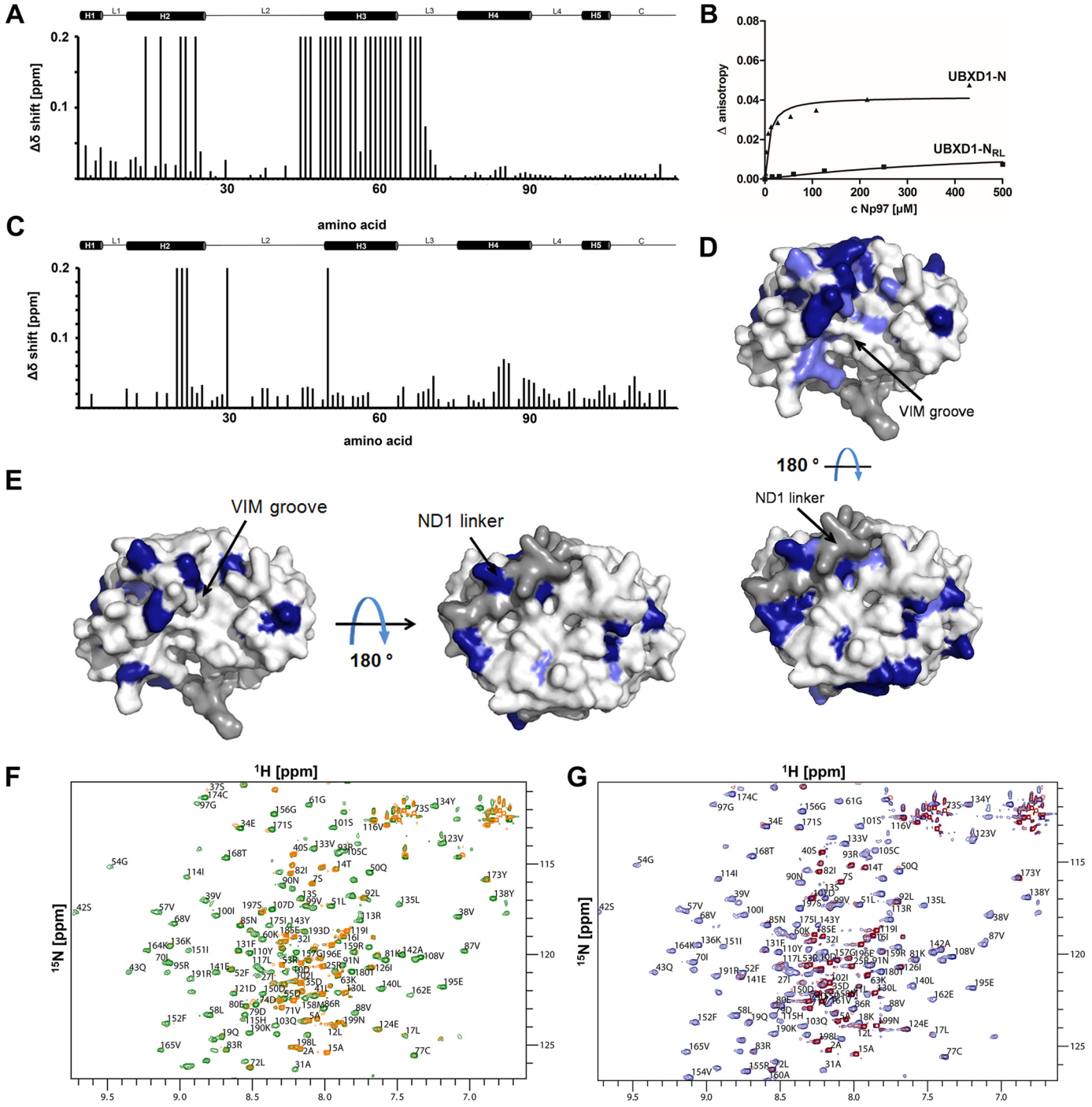

FIGURE 3. **Binding studies of UBXD1-N and p97-N.** *A*, shift difference map deduced from ^{1}H-^{15}N HSQC spectra of ^{15}N-labeled UBXD1-N in the absence and presence of p97-N. Amide resonances of residues that shift upon p97-N binding are represented by their corresponding shift difference values. Amide resonances of amino acids whose intensities vanish upon binding to p97-N are represented by *bars* with values of 0.2 ppm. *B*, fluorescence anisotropy binding studies of the UBXD1-N/p97-N interaction. Increasing amounts of p97-N were stepwise added to N-terminal Atto$_{594}$-labeled UBXD1-N(1–133)$_{WT}$ (▲) and UBXD1-N$_{R62A/L63A}$ (■). The K_D of p97-N/UBXD1-N was calculated to be 9 μM, and the K_D of p97-N/UBXD1-N$_{R62A/L63A}$ reflecting approximately the K_D of the new binding site between H1/H2 of UBXD1-N and the linker region (amino acids 187–200) of p97-N was calculated to be 580 μM. Graphs are representative. *C*, chemical shift difference map deduced from ^{1}H-^{15}N HSQC spectra of 200 μM UBXD1-N$_{R62A/L63A}$ in the absence and presence of 200 μM p97-N. Amide resonances of shifting residues are represented by their corresponding shift difference values. Amide resonances of amino acids whose intensities vanish upon binding to p97-N are represented by *bars* with values of 0.2 ppm. The mutation (R62A/L63A) of the VIM in UBXD1-N leads to a loss of binding of UBXD1-N to p97-N throughout the VIM, whereas binding still occurs through amino acids of the N terminus of UBXD1 (Gly^{20}, Gln^{21}, Lys^{22}, and Lys^{30}). *D*, NMR signals of amino acids of p97-N that either shift (*light blue*) or decline in intensity (*dark blue*) upon binding of UBXD1(1–80) are mapped on the surface of the p97-N structure (extracted N-domain including the ND1 linker in *gray* from Protein Data Bank code 1E32). *E*, surface representation of p97 N-domain with UBXD1(1–80)$_{R62A/L63A}$-interacting residues labeled as in Fig. 3*D*. *F*, section of the ^{1}H-^{15}N HSQC of p97-N$_{R155H}$. Spectra of p97-N$_{R155H}$ are presented in the absence (*green*) and presence (*orange*) of UBXD1-N(1–80). Intensities of p97-N signals from the random coil region (7.7–8.3 ppm) decrease after binding of UBXD1-N, whereas the complex precipitates immediately. *G*, section of the ^{1}H-^{15}N HSQC of p97-N$_{R95G}$. Spectra of p97-N$_{R95G}$ are presented in the absence (*blue*) and in the presence (*red*) of UBXD1-N(1–80). Intensities of p97-N signals from the random coil region (7.7–8.3 ppm) decrease after binding of UBXD1-N, whereas the complex precipitates after 1 day.

signals belonging to this region disappeared in the ^{1}H-^{15}N HSQC spectrum upon addition of p97-N, whereas residues Ala^{57}, Ala^{70}, and Trp^{71} showed only marginal chemical shifts changes. These observations suggest the direct involvement of the VIM in binding the N-domain of p97. Moreover, the stretch of interacting residues (27 amino acids) in UBXD1-N was much more extended compared with the general definition of the 10-amino acid containing VIM based on bioinformatics analysis of VIM-containing p97 cofactors (23). Most of the signals with decreased intensities belong to residues of H3 containing the VIM, whereas signals with only chemical shift changes are concentrated in H1/H2. Signal intensity loss indicates that the dynamics of complex formation is within the intermediate to slow exchange regime on the NMR time scale, pointing to high affinity binding constants of corresponding binding partners (K_D values in the lower μM to nM range). Changes in chemical shifts indicate that the exchange between bound and unbound conformations is within the fast exchange regime on the NMR time scale, which usually belongs to low affinity interactions (K_D values in the higher μM to mM range). Therefore, we concluded that the VIM and flanking residues (disappearing signals already at molar ratios of 0.2:1) bind p97-N with a higher affinity than H1/H2 (small shifts at molar ratios up to 1:5). For confirmation, the affinity of p97-N to UBXD1-N was calculated by fluorescence anisotropy to be 9 μM, which is in accordance with published data (32) (Fig. 3*B*). The affinity for the newly identified binding region of H1/H2 was investigated using the UBXD1-N mutant R62A/L63A, which is known to interrupt the interaction between the VIM and p97-N (23). Fluorescence anisotropy studies revealed that H1/H2 bound p97-N with a K_D of about 580 μM independently of the VIM (Fig. 3*B*). This is in accordance with the observation that only signals of residues belonging to H1/H2 decreased in their intensity and/or showed chemical shift changes in a corresponding ^{1}H-^{15}N HSQC titration experiment using the UBXD1-$N_{R62A/L63A}$ mutant (Fig. 3*C*). Hence, our results confirm the presence of a high affinity binding motif (VIM) within UBXD1-N, but moreover, they provide evidence for the existence of an additional low affinity binding site.

To identify the two UBXD1-N binding epitopes on p97-N, several concentrations of UBXD1-N(1–80) (to keep the molecular weight of the binding complex as low as possible) were added gradually to ^{15}N-labeled p97-N up to a molar ratio of 1:5, respectively. The corresponding chemical shift changes of the amide signals of p97-N were monitored by ^{1}H-^{15}N HSQC spectra (50 mM KP_i, pH 7.2). Upon binding of UBXD1-N, the intensities or chemical shifts of 48 NH signals changed. The corresponding residues were mapped onto the surface of the p97-N crystal structure including the ND1 linker (extracted from Protein Data Bank code 1E32) to visualize the binding areas (Fig. 3*D*). Two binding interfaces could be identified. The first interface comprises residues from the hydrophobic VIM-binding groove between the two subdomains of p97-N and neighboring residues (Val^{38}–Gln^{43}, Gly^{54}, Thr^{56}, Val^{88}, Val^{87}, Tyr^{138}–Tyr^{143}, Ile^{151}–Arg^{155}, Ile^{175}–Ile^{182}, and Cys^{105}–Gly^{111}). The second interface is composed of the linker region connecting the N-domain to the D1 domain of p97 and of amino acids located in close proximity on the surface of p97-N to this linker (Arg^{93}, Leu^{117}, Gly^{156}, and Cys^{184}–Glu^{195}). To specify which interface of p97-N is bound either by H1/H2 or by the VIM of UBXD1-N, the UBXD1-$N_{R62A/L63A}$ mutant was added to ^{15}N-labeled p97-N up to a molar ratio of 1:5, respectively. Upon binding of UBXD1-$N_{R62A/L63A}$, the intensities and chemical shifts of 26 NH signals were perturbed in the corresponding ^{1}H-^{15}N HSQC spectra. Most of the amino acids reside within the ND1 linker or within its neighborhood on the surface of p97-N (Gln^{50}, Lys^{60}, Ser^{73}, Arg^{93}, Ser^{101}, Leu^{117}, Gly^{156}/Gly^{157}, Cys^{184}, Lys^{190}, and Glu^{195} as well as Ile^{119}, Asn^{130}, and Asn^{199}, which are not bound by the wild type; Fig. 3*E*). Additionally, some amino acids were affected that are not clustered and are spread over the surface (Val^{39}–Gln^{43}, Asp^{55}, Leu^{58}, Cys^{105}, Leu^{140}, Tyr^{143}, and Thr^{168}). Thus, we conclude that the ND1 linker of p97 is preferably the binding region for H1/H2 of UBXD1-N, whereas the VIM binds the VIM groove between the two subdomains of p97-N.

The binding studies described above revealed the involvement of residues within p97-N that are mutated in patients with inclusion body myopathy associated with Paget disease of bone and frontotemporal dementia (Arg^{93}, Arg^{155}, and Arg^{191}). To investigate the influence of these mutations on binding of UBXD1-N to p97-N, increasing amounts of UBXD1-N(1–80) wild type were added to a molar ratio up to 1:1 to ^{15}N-labeled mutant p97-N_{R155H} (Fig. 3*F*) as well as ^{15}N-labeled mutant p97-N_{R95G} (Fig. 3*G*). However, the unspecific disappearance of signals in both spectra and an instant precipitate of p97-N_{R155H} and 1 day later of p97-N_{R95G} occurring within the sample suggest unspecific interaction and subsequent aggregation of the corresponding complexes, which precluded further analysis.

UBXD1-N Interacts with the D1D2 Barrel of p97—In addition to the binding sites observed for p97-N in the N terminus of UBXD1, UBXD1-N also bound to the D1D2 barrel of p97 with an affinity of 270 μM as demonstrated by fluorescence anisotropy measurements (Fig. 4*A*). Intriguingly, the binding of UBXD1-N to the p97-D1D2 barrel seems to be nucleotide-independent as the presence of ATP does not have an effect on the K_D value (270 $\pm$ 63 μM for ADP-bound *versus* 251 $\pm$ 53 μM for ATP-bound). An interaction between cofactors and the D1D2 domain of p97 has not been described so far. To study this interaction further, several concentrations of soluble p97-D1D2 protein were added to ^{15}N-labeled UBXD1-N up to a molar ratio of 1:1, respectively. The corresponding chemical shift and intensity changes of the amide signals of UBXD1-N were monitored by ^{1}H-^{15}N HSQC spectra (Fig. 4*B*). Upon titration of p97-D1D2 to UBXD1-N, the intensity of 38 amide signals decreased significantly, indicating a specific interaction of both proteins. The interacting residues are clearly concentrated in two stretches of UBXD1-N. Thereby, p97-D1D2 binds preferably H1/L1 (Phe^{4}, Phe^{5}, Gln^{7}, Phe^{8}, Asp^{11}–Phe^{14}, and Ala^{17}) and H3/H4 (Glu^{51}–Gln^{53}, Ala^{55}–Gln^{65}, Gln^{67}, Arg^{69}–Gly^{72}, Thr^{78}–Arg^{80}, Val^{83}–Glu^{86}, and Gln^{88}–Glu^{90}) including the known VIM (Ala^{52}–Arg^{62}) and its flanking residues. In comparison with p97-N, p97-D1D2 binds the N-terminal region of H1/H2 (H1/H2 Met^{1}–Ser26 and 9 affected residues within Phe^{4}–Ala^{17}), whereas p97-N is primarily bound to H2 (H2 Ala^{10}–Ser^{26} and 6 disappearing signals between Phe^{14} and Glu^{25}). As shown, the VIM interacts with the N-domain as well

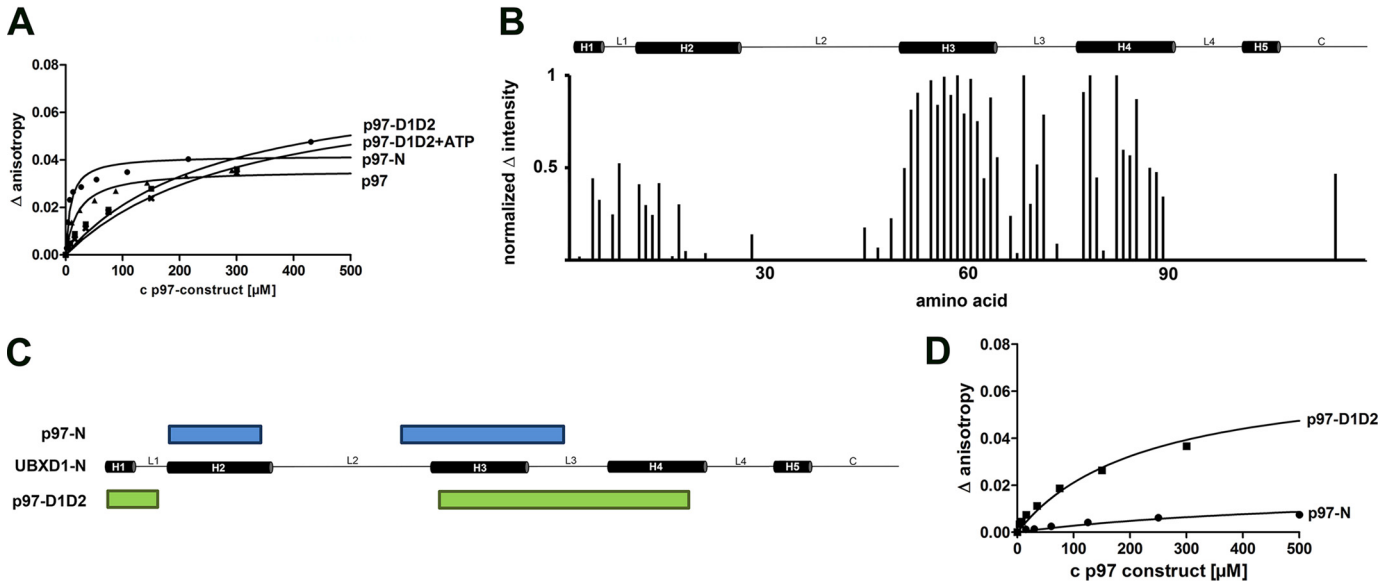

FIGURE 4. **Binding studies of UBXD1-N and p97-D1D2.** *A*, fluorescence anisotropy binding studies of $Atto_{594}$-labeled UBXD1-N with increasing amounts of different p97 constructs. K_D values of UBXD1-N binding to p97 constructs were calculated to be 9 μM for p97-N (●), 270 μM for p97-D1D2 (■), 251 μM for p97-D1D2 + ATP (×; 2 mM ATP; normalized to p97-D1D2), and 21 μM for full-length p97 (▲). Graphs are representative. *B*, intensity differences calculated from amide resonances of ^{1}H-^{15}N HSQC spectra of 100 μM ^{15}N-labeled UBXD1-N in the absence and presence of 200 μM p97-D1D2. Binding of p97-D1D2 to UBXD1-N occurs in H1/L1 and H3/L3/H4. *C*, a comparison of the binding epitopes on UBXD1-N of p97-N (*blue*) and p97-D1D2 (*green*) reveals a similar binding mode with overlap of interacting residues in the N terminus and the VIM. *D*, fluorescence anisotropy binding studies of N-terminal $Atto_{594}$-labeled UBXD1-$N_{R62A/L63A}$ by stepwise addition of p97-N (▲) or p97-D1D2 (■). The K_D for p97-N was calculated to be 580 μM, and the K_D for p97-D1D2 was calculated to be 226 μM. Graphs are representative.

as with the D1D2 barrel of p97, but p97-N preferably binds the N-terminal region of the VIM, whereas the D1D2 barrel interacts with the C-terminal part of the VIM (Fig. 4*C*), suggesting a different binding mechanism of UBXD1-N to the N-domain and the D1D2 barrel of p97. This hypothesis is also in line with fluorescence anisotropy measurements of a UBXD1 mutant lacking a functional VIM (Fig. 4*D*). Although the binding of UBXD1-$N_{R62A/L63A}$ to p97-N is significantly reduced due to the mutation, it remains similar to the p97-D1D2 construct.

UBXD1-N Inhibits the ATPase Activity of p97 and Fixes the N Domain of p97 in an Altered Conformation When Compared with p47—Our studies indicate that the isolated N terminus of UBXD1 binds in a similar region on p97-N as the cofactor p47. Because p47 is known to inhibit the p97 ATPase activity (33), we tested the ATPase activity of p97 in the presence of UBXD1-N using an NADH-coupled ATPase assay (Fig. 5*A*). UBXD1-N reduced the ATPase activity of p97 in a concentration-dependent manner to 7.27 μmol of ATP/mg of p97/h (41%; K_i = 8 nM) similar to p47 (reduction to 5.59 μmol of ATP/mg of p97/h; 31%; K_i = 7 nM). In contrast, the addition of Tris buffer did not have any significant effect on the p97 ATPase activity.

For the p97·p47 complex, EM-based structure analysis indicated that the N-domain of p97 is held in an "up" conformation by p47 (34). Because our data indicated that the UBXD1-N interacts with both the N-domain and the D1D2 domain of p97, we wondered whether UBXD1-N constrains p97-N in the same conformation. To investigate various conformations caused by either p47 or UBXD1-N, p97 was degraded by limited proteolysis using trypsin (Fig. 5, *B* and for time courses *C*). Untreated p97 displays a prominent band on SDS-PAGE at roughly 100 kDa (*lane 1*). Upon digestion, two major bands of ~55 and 75 kDa (*lane 2*) appeared (negative control). The band patterns in the presence of both the cofactor p47 (stoichiometry of 3:6 (p47:p97), *lane 3*) and the non-hydrolyzable substrate analogue ATPγS (*lane 4*) are comparable with the negative control (*lane 2*). Because the binding of p47 leads to a fixation of the p97 N-domain in an upper position (34), the corresponding conformational changes made the linker between the domains of p97 accessible for enzymatic proteolysis by trypsin. Only bands corresponding to the rigid and protected domains of p97 are left. The band for p47 below 55 kDa disappears due to partial degradation by trypsin, whereas another band at 25 kDa appears. LC-MS/MS analysis identified this band as parts of p47 containing the Shp1-eyc-p47 domain (SEP) as well as the p97-N binding UBX domain (data not shown). A modified UBXD1-N construct (amino acids 32–133, R62A/L63A), which does not bind the VIM groove of p97-N or the ND1 linker but still interacts with p97-D1D2, fails to protect p97 against proteolysis (*lane 6*). In this case, a similar band pattern is observed as in the presence of p47 or ATPγS (*lanes 3* and *4*). Only UBXD1-N_{WT}, which binds p97-N as well as p97-D1D2, is able to partially protect full-length p97 from proteolysis by trypsin, resulting in a different band pattern (100, 70, and 20 kDa; *lane 5*). The different band pattern of p97 after limited proteolysis in the presence of UBXD1-N or p47 indicates an altered conformation of the p97 hexamer. Additionally, temperature stability experiments confirmed a higher melting temperature of p97 in the presence of UBXD1-N (>88 °C) in comparison with that in its absence (68 °C) or in the presence of its substrate analogue ATPγS (71 °C) (Fig. 5*D*). Due to the high Trp content of p47 (13 Trp residues) compared with p97 (3 Trp residues), it was not possible to perform the thermal stability assay in the presence of the cofactor p47. The altered proteolysis pattern and the high

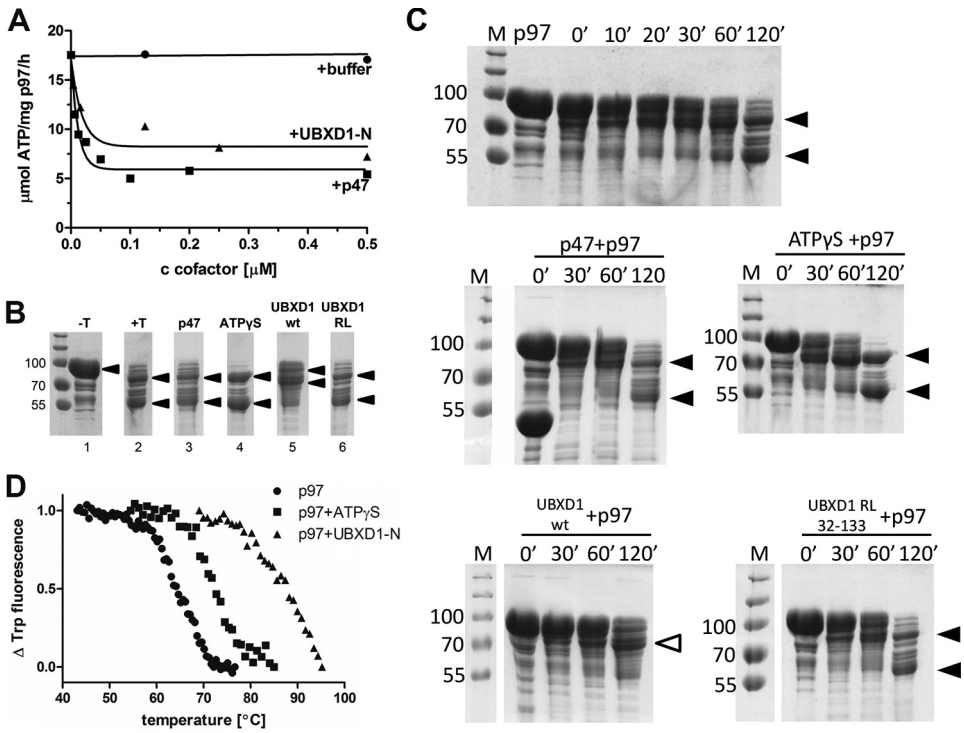

FIGURE 5. **Evidence for conformational changes of p97 during UBXD1-N binding.** *A*, ATPase activity of p97 (●) is reduced concentration-dependently by either p47 (■; 31%) or UBXD1-N (▲; 41%). Graphs are representative. *B*, limited proteolysis of p97 (10 μM) using trypsin (*T*) in the absence of any cofactor (*lane 2*) or in the presence of either p47 (5 μM; *lane 3*), ATPγS (5 mM; *lane 4*), UBXD1-N_{WT} (10 μM; *lane 5*), or UBXD1-N(32–133)$_{R62A/L63A}$ (*RL*; 10 μM; *lane 6*). *C*, limited proteolysis at time points as indicated for p97, p47 and p97, ATPγS and p97, UBXD1-N_{WT} and p97, and UBXD1-$N_{R62A/L63A}$ and p97. Differences in the band pattern after digestion of p97 with trypsin are indicated by *arrowheads*. *D*, stability of p97 (●) or p97 in the presence of the non-hydrolyzable substrate ATPγS (■) or UBXD1-N(1–133) (▲) was monitored by following the intrinsical tryptophan fluorescence during stepwise heating of the samples. Melting of p97 in the absence of any compound occurs at 68 °C. Binding of either ATPγS or UBXD1-N led to higher melting temperatures of 71 and >88 °C, respectively, pointing toward higher stability of p97. Data are presented as the ratio between the highest Trp fluorescence at 328 nm and the fluorescence at the specific temperature. *Lane M*, molecular weight markers; ′, minutes.

increase of the p97 melting temperature in the presence of UBXD1-N indicate that UBXD1-N fixes p97-N in a conformation that is different from the p47-related up conformation. This altered conformation seems to restrict the flexibility of the N-domain and the linker regions of p97 required for the p97 ATPase activity, explaining the observed influence of UBXD1-N on the p97 ATPase activity.

Discussion

Among the p97 cofactors, UBXD1 is particular because it has a complex interaction mode with p97 that is specifically affected by disease-associated mutations in p97 (14, 23). In this study, we report detailed data on the structure and binding mechanism of the critical isolated UBXD1-N moiety. Our NMR and CD spectroscopic analyses of UBXD1-N have elucidated the absence of a stable tertiary fold and the presence of stretches of mainly transient secondary structural elements with exception of the VIM. Structural predictions using the Predictor of Natural Disordered Regions algorithm (Fig. 6*A*) support the notion that even in full-length UBXD1 no rigid three-dimensional topology is present for the N-terminal region. The high number of disorder-supporting residues (68%; namely Ala, Arg, Gly, Gln, Ser, Glu, Lys, and Pro (35, 36)) and the presence of a considerable number of charged amino acids (26%) argues for an enhanced hydrodynamic radius of UBXD1-N, leading to the short elution time in size exclusion chromatography. Taken together, these features are consistent with the interpretation that the N terminus of UBXD1 can be classified as an overall intrinsically disordered region of UBXD1. Intrinsically disordered proteins have attracted much attention during the last two decades, and thus their general regulatory role in signaling and controlling pathways is widely accepted (37–40). The unique binding properties and the regulative potential of intrinsically disordered regions in proteins were recently discovered to appear also in cofactors of p97 (41–43). Moreover, proteins that are involved in p97-related pathways such as endoplasmic reticulum-associated protein degradation (44) and the ubiquitination system for protein degradation also contain unstructured amino acid stretches with regulative roles (45).

The flexible N-terminal region of UBXD1 contains the well defined α-helical VIM, which is known to bind the groove between the two subdomains of p97-N (23, 32). This interaction was also confirmed by our NMR spectroscopic studies at the atomic level. However, consistent with our cell-based assays monitoring UBXD1 localization to p97 on CAV1 endosomes, our structural studies revealed a more complex binding mechanism than noted previously (23). We discovered a new interaction site on H1/H2 in UBXD1-N that binds the ND1 linker of p97 independently from the VIM. The H1/H2 binding region is α-helical and conserved among several species but unique for the UBXD1 cofactor. UBXD1 has recently been shown to also bind a population of ERGIC-53 at the plasma membrane with

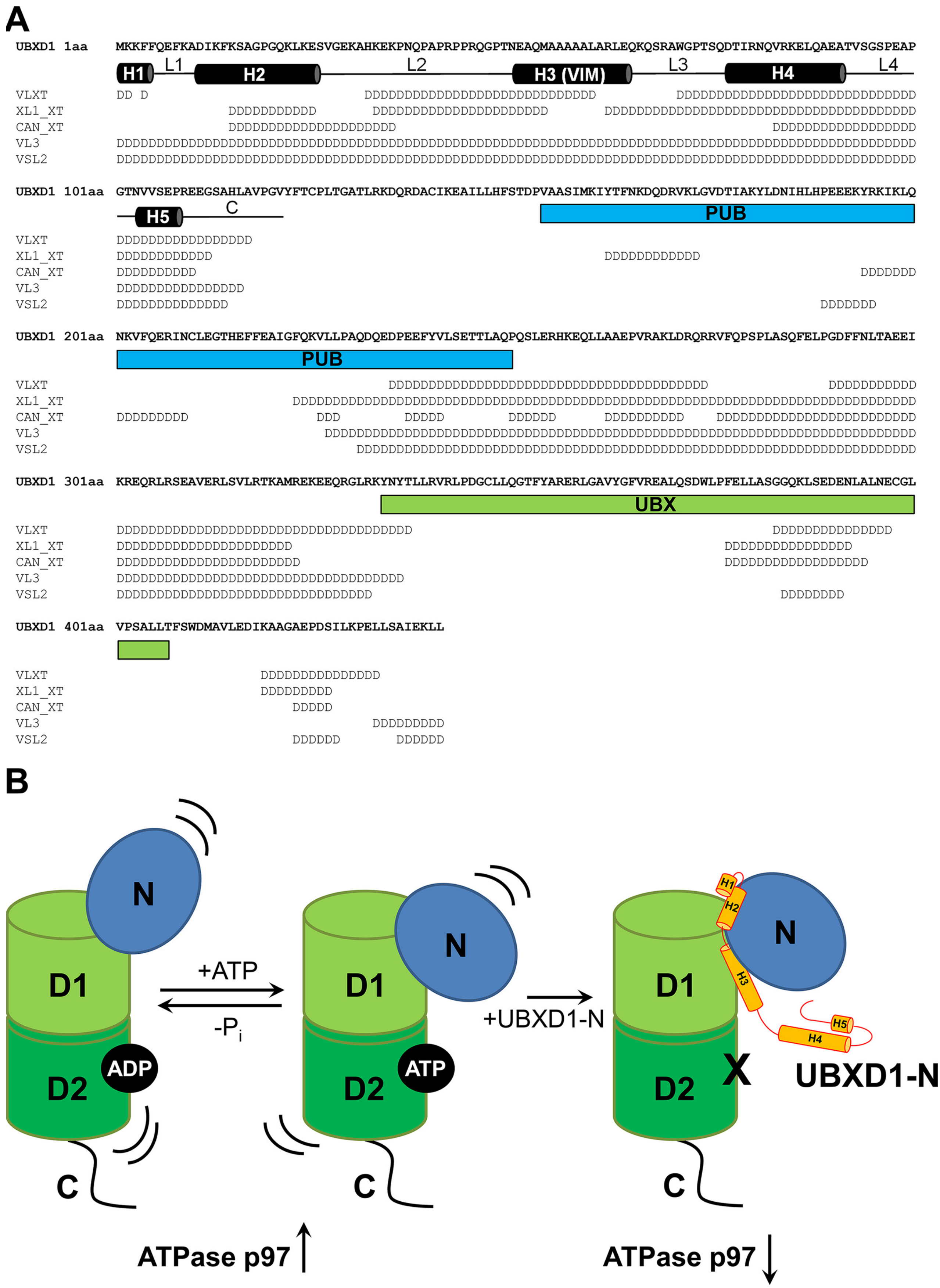

the very N-terminal amino acids (46). Intriguingly, this region overlaps with the H1/H2 binding site for p97, and therefore it would be interesting to clarify whether these differential interactions of UBXD1 represent alternative functions or whether they are functionally linked. Additionally, both binding regions of UBXD1-N are also involved in the interaction with the D1D2 barrel of p97. The binding of p97-N and -D1D2 seems to occur simultaneously because there is only a partial overlap of binding epitopes on UBXD1-N. Although we were not able to identify the binding interface on p97-D1D2 exactly, we assume that binding occurs to the D1 domain as UBXD1-N binds residues of the interface between the N-domain and D1 domain as well as the linker between the N-domain and the D1 domain of p97 (Fig. 6*B*).

The intrinsically disordered region characteristic of UBXD1-N and the absence of a defined tertiary structure may affect the ability of the protein to properly fit into the polyepitopic interface region on the p97 protein. In fact, we suggest that the intrinsic flexibility of UBXD1-N may be a structural requirement for targeting the VIM groove of p97-N while simultaneously grabbing the flexible ND1 linker and the D1D2 barrel at a very far distance. Of note, in a number of cofactors, short p97-binding motifs lie in regions without defined domain structure for example in UBE4B, small VCP-interacting protein, VCP-interacting membrane protein, Hrd1, and autocrine motility factor receptor (43, 47–50). Moreover, the VIM protein small VCP-interacting protein was also shown to bind the ND1 linker (32, 41). Based on our new data on UBXD1-N, we therefore propose that polyvalent binding of intrinsically disordered regions containing short p97-binding motifs is a more general feature of a number of p97 cofactors and thereby defines a subclass of cofactors.

Two additional observations in this study are consistent with the notion that UBXD1-N intercalates in a complex manner and possibly affects the flexibility of the N-domain. First, we show that UBXD1-N binding to p97 changes the protease sensitivity of p97 in comparison with p47. These changes can either occur from protection of proteolysis sites or from domain reorientation. We assume that the changed protease pattern results from domain reorientation because the proteolysis pattern of free p97 does not change upon binding of the cofactor p47, although UBXD1-N and p47 share a similar binding site on p97-N. p47, however, is known to lock p97-N in an up conformation. Considering the additional binding site of UBXD1-N on the D1D2 barrel and the fact that only two extreme positions of the p97 N-domain are realized within the hexamer, it is reasonable to assume that UBXD1-N locks p97-N in a "down" conformation toward the D1D2 barrel. Another indication for a compaction of p97·UBXD1-N is the UBXD1-N-mediated melting temperature increase of p97 (about 20 °C). Because a long intrinsically disordered protein chain should lead to a strong positive $-T{\cdot}\Delta S$ contribution to the Gibbs free enthalpy, such an unfavorable contribution can be overcompensated by additional new binding sites formed in the presence of UBXD1-N by intradomain/domain interaction as postulated to occur upon formation of the down conformation. Second and connected to the first, UBXD1-N binding to p97 inhibits its ATPase activity. Previous reports have established that p97-N motion relative to the D1 plane is coupled to ATPase activity and that locking the N-domain in a down position inhibits ATPase activity (11). Moreover, the contact between the N-domain and the D1 domain is important for the allosteric communication between substrate adaptor binding and ATPase domains (9, 11, 51). We therefore speculate that binding of UBXD1-N into the p97-ND1 interface may prevent p97-N motion and thus inhibit ATPase activity (Fig. 6*B*). An analogous explanation has been suggested for the inhibitory effect of the p47 cofactor on the ATPase activity; only in this case, p47 locks the N-domain in an up position (33, 34). This, in turn, is consistent with the differential effect on protease sensitivity compared with UBXD1-N in our experiments. Following this idea of the intrinsically disordered region being a prerequisite for tethering the p97 domains and fixing them in a compact formation, the intrinsically disordered region characteristics are consecutively responsible for the decrease of p97 ATPase activity. Previously, N-terminally tagged full-length UBXD1 was reported to have no effect on p97 ATPase activity (52). We assume that the isolated UBXD1-N moiety is decoupled from regulatory elements of the protein and that pausing p97-N motions can only be a transient step in the context of the p97-mediated substrate protein remodeling reaction. Conversely, the specific inhibition of the ATPase activity of p97 by the N terminus of UBXD1 supports the notion that the intrinsic features of UBXD1-N also apply in the context of the full-length protein. Although the substoichiometric inhibition of p97 by UBXD1-N is quite unusual, such phenomena have already been described for oligomerizing protomers (53–57). Therefore, we hypothesize a kind of sustainability of the UBXD1-N interaction with the p97 hexamer. In any case, the specific mode of interaction between UBXD1-N and p97 points to a distinct modulation of the p97-mediated segregation mechanism particularly required in UBXD1-regulated processes as opposed to p47- or Ufd1-Npl4-regulated reactions (1, 58).

The binding mechanism of UBXD1-N to p97 may also be relevant for p97-associated diseases. Disease-causing mutations all lie at the critical interface between the p97 N-domain and D1 domain and are believed to affect their allosteric communication (4). Crucially, we show here that UBXD1-N binding occurs at this interface and even involves residues mutated in the disease. Moreover, we showed earlier that binding of UBXD1, but not p47 or Ufd1-Npl4, which have different binding epitopes on p97, to disease-associated p97 mutants is specifically reduced (14). Consistently, compromised sorting of caveolin-1 is a dominant feature in cells expressing disease-

FIGURE 6. **Model of the binding interface of UBXD1-N and p97.** *A*, Predictor of Natural Disordered Regions analysis of the N terminus of UBXD1 in the context of the full-length UBXD1 protein. *B*, ATP hydrolysis in the p97-D2 domain is coupled to motions of the N-domain via a chain of conformational changes involving the D1 domain and the ND1 linker of p97. Insertion of UBXD1-N into the ND1 interface is mediated by interaction with the N-domain, the ND1 linker, and parts of the D1D2 barrel of p97. As a result, the flexibility of the N-domain is restricted, and the ATPase activity of p97 is decreased. This mechanism may be transient in the context of a complex p97-mediated segregation reaction. The binding sites involve residues mutated in p97-associated disease, suggesting that effects on UBXD1-N binding may form the basis for the disease pathogenesis. *aa*, amino acid.

associated mutants of p97 (14). We therefore speculate that the intimate intercalation of UBXD1-N into the p97-ND1 interface constitutes the specific structural basis for the pathogenic mechanism observed in the case of p97 disease-associated mutations.

From our structural analysis of the isolated N terminus of UBXD1 and further biophysical binding studies with single domains of p97, we conclude that the UBXD1-N engages in polyvalent binding to several regions within the ND1 domain interface of p97. Our findings indicate that UBXD1-N intercalates into the p97-ND1 interface, thereby modulating the interdomain communication of p97 domains and hence inhibiting its ATPase activity in a similar way to p47. We propose that such a polyvalent binding mode is facilitated by the fact that UBXD1-N is highly flexible and/or intrinsically disordered and that this is a more general principle that defines a new subset of p97 cofactors containing short p97-binding motifs in regulatory disordered regions. Moreover, the facts that UBXD1-N interaction sites include those residues frequently mutated in patients with inclusion body myopathy associated with Paget disease of bone and frontotemporal dementia and that UBXD1 binding is affected in the disease model suggest that this particular binding mode also may have relevance for disease pathogenesis.

Author Contributions—Experiments were predominantly done by F. T. Cellular experiments were conducted by M. V., L. K., and H. K. A. M. contributed to NMR experiments. Ideas and conception of the work came from F. T., P. S. F., H. M., and P. B. The manuscript was written and revised by all authors. All authors have given approval to the final version of the manuscript.

Acknowledgment—We thank R. Pöhler for providing the p97 full-length protein.

References

1. Meyer, H., Bug, M., and Bremer, S. (2012) Emerging functions of the VCP/p97 AAA-ATPase in the ubiquitin system. *Nat. Cell Biol.* **14,** 117–123
2. Yamanaka, K., Sasagawa, Y., and Ogura, T. (2012) Recent advances in p97/VCP/Cdc48 cellular functions. *Biochim. Biophys. Acta* **1823,** 130–137
3. Ye, Y. (2006) Diverse functions with a common regulator: ubiquitin takes command of an AAA ATPase. *J. Struct. Biol.* **156,** 29–40
4. Meyer, H., and Weihl, C. C. (2014) The VCP/p97 system at a glance: connecting cellular function to disease pathogenesis. *J. Cell Sci.* **127,** 3877–3883
5. Ju, J. S., and Weihl, C. C. (2010) p97/VCP at the intersection of the autophagy and the ubiquitin proteasome system. *Autophagy* **6,** 283–285
6. Kloppsteck, P., Ewens, C. A., Förster, A., Zhang, X., and Freemont, P. S. (2012) Regulation of p97 in the ubiquitin-proteasome system by the UBX protein-family. *Biochim. Biophys. Acta* **1823,** 125–129
7. Stolz, A., Hilt, W., Buchberger, A., and Wolf, D. H. (2011) Cdc48: a power machine in protein degradation. *Trends. Biochem. Sci.* **36,** 515–523
8. Jentsch, S., and Rumpf, S. (2007) Cdc48 (p97): a "molecular gearbox" in the ubiquitin pathway? *Trends. Biochem. Sci.* **32,** 6–11
9. DeLaBarre, B., and Brunger, A. T. (2005) Nucleotide dependent motion and mechanism of action of p97/VCP. *J. Mol. Biol.* **347,** 437–452
10. Pye, V. E., Dreveny, I., Briggs, L. C., Sands, C., Beuron, F., Zhang, X., and Freemont, P. S. (2006) Going through the motions: the ATPase cycle of p97. *J. Struct. Biol.* **156,** 12–28
11. Niwa, H., Ewens, C. A., Tsang, C., Yeung, H. O., Zhang, X., and Freemont, P. S. (2012) The role of the N-domain in the ATPase activity of the mammalian AAA ATPase p97/VCP. *J. Biol. Chem.* **287,** 8561–8570
12. Müller, J. M., Deinhardt, K., Rosewell, I., Warren, G., and Shima, D. T. (2007) Targeted deletion of p97 (VCP/CDC48) in mouse results in early embryonic lethality. *Biochem. Biophys. Res. Commun.* **354,** 459–465
13. Watts, G. D., Wymer, J., Kovach, M. J., Mehta, S. G., Mumm, S., Darvish, D., Pestronk, A., Whyte, M. P., and Kimonis, V. E. (2004) Inclusion body myopathy associated with Paget disease of bone and frontotemporal dementia is caused by mutant valosin-containing protein. *Nat. Genet.* **36,** 377–381
14. Ritz, D., Vuk, M., Kirchner, P., Bug, M., Schütz, S., Hayer, A., Bremer, S., Lusk, C., Baloh, R. H., Lee, H., Glatter, T., Gstaiger, M., Aebersold, R., Weihl, C. C., and Meyer, H. (2011) Endolysosomal sorting of ubiquitylated caveolin-1 is regulated by VCP and UBXD1 and impaired by VCP disease mutations. *Nat. Cell Biol.* **13,** 1116–1123
15. Tresse, E., Salomons, F. A., Vesa, J., Bott, L. C., Kimonis, V., Yao, T. P., Dantuma, N. P., and Taylor, J. P. (2010) VCP/p97 is essential for maturation of ubiquitin-containing autophagosomes and this function is impaired by mutations that cause IBMPFD. *Autophagy* **6,** 217–227
16. Halawani, D., LeBlanc, A. C., Rouiller, I., Michnick, S. W., Servant, M. J., and Latterich, M. (2009) Hereditary inclusion body myopathy-linked p97/VCP mutations in the NH2 domain and the D1 ring modulate p97/VCP ATPase activity and D2 ring conformation. *Mol. Cell. Biol.* **29,** 4484–4494
17. Tang, W. K., and Xia, D. (2013) Altered intersubunit communication is the molecular basis for functional defects of pathogenic p97 mutants. *J. Biol. Chem.* **288,** 36624–36635
18. Weihl, C. C., Pestronk, A., and Kimonis, V. E. (2009) Valosin-containing protein disease: inclusion body myopathy with Paget's disease of the bone and fronto-temporal dementia. *Neuromuscul. Disord.* **19,** 308–315
19. Fernández-Sáiz, V., and Buchberger, A. (2010) Imbalances in p97 co-factor interactions in human proteinopathy. *EMBO Rep.* **11,** 479–485
20. Kern, M., Fernandez-Sáiz, V., Schäfer, Z., and Buchberger, A. (2009) UBXD1 binds p97 through two independent binding sites. *Biochem. Biophys. Res. Commun.* **380,** 303–307
21. Hayer, A., Stoeber, M., Ritz, D., Engel, S., Meyer, H. H., and Helenius, A. (2010) Caveolin-1 is ubiquitinated and targeted to intralumenal vesicles in endolysosomes for degradation. *J. Cell Biol.* **191,** 615–629
22. Kirchner, P., Bug, M., and Meyer, H. (2013) Ubiquitination of the N-terminal region of caveolin-1 regulates endosomal sorting by the VCP/p97 AAA-ATPase. *J. Biol. Chem.* **288,** 7363–7372
23. Stapf, C., Cartwright, E., Bycroft, M., Hofmann, K., and Buchberger, A. (2011) The general definition of the p97/valosin-containing protein (VCP)-interacting motif (VIM) delineates a new family of p97 cofactors. *J. Biol. Chem.* **286,** 38670–38678
24. Grum, D., Franke, S., Kraff, O., Heider, D., Schramm, A., Hoffmann, D., and Bayer, P. (2013) Design of a modular protein-based MRI contrast agent for targeted application. *PLoS One* **8,** e65346
25. Isaacson, R. L., Pye, V. E., Simpson, P., Meyer, H. H., Zhang, X., Freemont, P. S., and Matthews, S. (2007) Detailed structural insights into the p97-Npl4-Ufd1 interface. *J. Biol. Chem.* **282,** 21361–21369
26. Ayed, A., Mulder, F. A., Yi, G. S., Lu, Y., Kay, L. E., and Arrowsmith, C. H. (2001) Latent and active p53 are identical in conformation. *Nat. Struct. Biol.* **8,** 756–760
27. Compton, L. A., and Johnson, W. C., Jr. (1986) Analysis of protein circular dichroism spectra for secondary structure using a simple matrix multiplication. *Anal. Biochem.* **155,** 155–167
28. Sreerama, N., and Woody, R. W. (2000) Estimation of protein secondary structure from circular dichroism spectra: comparison of CONTIN, SELCON, and CDSSTR methods with an expanded reference set. *Anal. Biochem.* **287,** 252–260
29. Johnson, W. C. (1999) Analyzing protein circular dichroism spectra for accurate secondary structures. *Proteins* **35,** 307–312
30. Wishart, D. S., Bigam, C. G., Holm, A., Hodges, R. S., and Sykes, B. D. (1995) ^{1}H, ^{13}C and ^{15}N random coil NMR chemical shifts of the common amino acids. I. Investigations of nearest-neighbor effects. *J. Biomol. NMR* **5,** 67–81
31. Combet, C., Blanchet, C., Geourjon, C., and Deléage, G. (2000) NPS@: network protein sequence analysis. *Trends. Biochem. Sci.* **25,** 147–150

32. Hänzelmann, P., and Schindelin, H. (2011) The structural and functional basis of the p97/valosin-containing protein (VCP)-interacting motif (VIM): mutually exclusive binding of cofactors to the N-terminal domain of p97. *J. Biol. Chem.* **286,** 38679–38690
33. Meyer, H. H., Kondo, H., and Warren, G. (1998) The p47 co-factor regulates the ATPase activity of the membrane fusion protein, p97. *FEBS Lett.* **437,** 255–257
34. Beuron, F., Dreveny, I., Yuan, X., Pye, V. E., McKeown, C., Briggs, L. C., Cliff, M. J., Kaneko, Y., Wallis, R., Isaacson, R. L., Ladbury, J. E., Matthews, S. J., Kondo, H., Zhang, X., and Freemont, P. S. (2006) Conformational changes in the AAA ATPase p97-p47 adaptor complex. *EMBO J.* **25,** 1967–1976
35. Williams, R. M., Obradovi, Z., Mathura, V., Braun, W., Garner, E. C., Young, J., Takayama, S., Brown, C. J., and Dunker, A. K. (2001) The protein non-folding problem: amino acid determinants of intrinsic order and disorder. *Pac. Symp. Biocomput.* **2001,** 89–100
36. Romero, P., Obradovic, Z., Li, X., Garner, E. C., Brown, C. J., and Dunker, A. K. (2001) Sequence complexity of disordered protein. *Proteins* **42,** 38–48
37. Uversky, V. N. (2013) A decade and a half of protein intrinsic disorder: biology still waits for physics. *Protein Sci.* **22,** 693–724
38. Tompa, P. (2012) Intrinsically disordered proteins: a 10-year recap. *Trends Biochem. Sci.* **37,** 509–516
39. Dyson, H. J., and Wright, P. E. (2005) Intrinsically unstructured proteins and their functions. *Nat. Rev. Mol. Cell Biol.* **6,** 197–208
40. Dunker, A. K., Obradovic, Z., Romero, P., Garner, E. C., and Brown, C. J. (2000) Intrinsic protein disorder in complete genomes. *Genome Inform. Ser. Workshop Genome Inform.* **11,** 161–171
41. Wu, J., Peng, D., Voehler, M., Sanders, C. R., and Li, J. (2013) Structure and expression of a novel compact myelin protein—small VCP-interacting protein (SVIP). *Biochem. Biophys. Res. Commun.* **440,** 173–178
42. Liu, J., Li, F., and Rozovsky, S. (2013) The intrinsically disordered membrane protein selenoprotein S is a reductase *in vitro*. *Biochemistry* **52,** 3051–3061
43. Christensen, L. C., Jensen, N. W., Vala, A., Kamarauskaite, J., Johansson, L., Winther, J. R., Hofmann, K., Teilum, K., and Ellgaard, L. (2012) The human selenoprotein VCP-interacting membrane protein (VIMP) is non-globular and harbors a reductase function in an intrinsically disordered region. *J. Biol. Chem.* **287,** 26388–26399
44. Xu, Y., Liu, Y., Lee, J. G., and Ye, Y. (2013) A ubiquitin-like domain recruits an oligomeric chaperone to a retrotranslocation complex in endoplasmic reticulum-associated degradation. *J. Biol. Chem.* **288,** 18068–18076
45. Frye, J. J., Brown, N. G., Petzold, G., Watson, E. R., Grace, C. R., Nourse, A., Jarvis, M. A., Kriwacki, R. W., Peters, J. M., Stark, H., and Schulman, B. A. (2013) Electron microscopy structure of human APC/C(CDH1)-EMI1 reveals multimodal mechanism of E3 ligase shutdown. *Nat. Struct. Mol. Biol.* **20,** 827–835
46. Haines, D. S., Lee, J. E., Beauparlant, S. L., Kyle, D. B., den Besten, W., Sweredoski, M. J., Graham, R. L., Hess, S., and Deshaies, R. J. (2012) Protein interaction profiling of the p97 adaptor UBXD1 points to a role for the complex in modulating ERGIC-53 trafficking. *Mol. Cell Proteomics* **11,** M111.016444
47. Liu, S., Fu, Q. S., Zhao, J., and Hu, H. Y. (2013) Structural and mechanistic insights into the arginine/lysine-rich peptide motifs that interact with P97/VCP. *Biochim. Biophys. Acta* **1834,** 2672–2678
48. Li, H. Y., Zheng, X. M., Che, M. X., and Hu, H. Y. (2012) A redox-sensitive luciferase assay for determining the localization and topology of endoplasmic reticulum proteins. *PLoS One* **7,** e35628
49. Tanaka, N., Haga, A., Naba, N., Shiraiwa, K., Kusakabe, Y., Hashimoto, K., Funasaka, T., Nagase, H., Raz, A., and Nakamura, K. T. (2006) Crystal structures of mouse autocrine motility factor in complex with carbohydrate phosphate inhibitors provide insight into structure-activity relationship of the inhibitors. *J. Mol. Biol.* **356,** 312–324
50. Benirschke, R. C., Thompson, J. R., Nominé, Y., Wasielewski, E., Juranić, N., Macura, S., Hatakeyama, S., Nakayama, K. I., Botuyan, M. V., and Mer, G. (2010) Molecular basis for the association of human E4B U box ubiquitin ligase with E2-conjugating enzymes UbcH5c and Ubc4. *Structure* **18,** 955–965
51. Tang, W. K., Li, D., Li, C. C., Esser, L., Dai, R., Guo, L., and Xia, D. (2010) A novel ATP-dependent conformation in p97 N-D1 fragment revealed by crystal structures of disease-related mutants. *EMBO J.* **29,** 2217–2229
52. Madsen, L., Andersen, K. M., Prag, S., Moos, T., Semple, C. A., Seeger, M., and Hartmann-Petersen, R. (2008) Ubxd1 is a novel co-factor of the human p97 ATPase. *Int. J. Biochem. Cell Biol.* **40,** 2927–2942
53. Gersch, M., Famulla, K., Dahmen, M., Göbl, C., Malik, I., Richter, K., Korotkov, V. S., Sass, P., Rübsamen-Schaeff, H., Madl, T., Brötz-Oesterhelt, H., and Sieber, S. A. (2015) AAA+ chaperones and acyldepsipeptides activate the ClpP protease via conformational control. *Nat. Commun.* **6,** 6320
54. Mustafi, S. M., Garai, K., Crick, S. L., Baban, B., and Frieden, C. (2010) Substoichiometric inhibition of Aβ(1–40) aggregation by a tandem Aβ(40-1-Gly8-1-40) peptide. *Biochem. Biophys. Res. Commun.* **397,** 509–512
55. Orosz, F., Santamaría, B., Ovádi, J., and Aragón, J. J. (1999) Phosphofructokinase from *Dictyostelium discoideum* is a potent inhibitor of tubulin polymerization. *Biochemistry* **38,** 1857–1865
56. Plenge-Tellechea, F., Soler, F., and Fernandez-Belda, F. (1997) On the inhibition mechanism of sarcoplasmic or endoplasmic reticulum Ca^{2+}-ATPases by cyclopiazonic acid. *J. Biol. Chem.* **272,** 2794–2800
57. Smith, S. L., Jennett, R. B., Sorrell, M. F., and Tuma, D. J. (1992) Substoichiometric inhibition of microtubule formation by acetaldehyde-tubulin adducts. *Biochem. Pharmacol.* **44,** 65–72
58. Uchiyama, K., and Kondo, H. (2005) p97/p47-mediated biogenesis of Golgi and ER. *J. Biochem.* **137,** 115–119

The N-terminal Region of the Ubiquitin Regulatory X (UBX) Domain-containing Protein 1 (UBXD1) Modulates Interdomain Communication within the Valosin-containing Protein p97

Franziska Trusch, Anja Matena, Maja Vuk, Lisa Koerver, Helene Knævelsrud, Paul S. Freemont, Hemmo Meyer and Peter Bayer

J. Biol. Chem. 2015, 290:29414-29427.
doi: 10.1074/jbc.M115.680686 originally published online October 16, 2015